TECHNISCHE MECHANIK, 32, 2-5, (2012), 130 – 145
submitted: November 1, 2011

Experiments and Modelling of the Cyclic Behaviour of Haynes 282

R. Brommesson, M. Ekh

In this contribution the mechanical behaviour of the Ni-based superalloy Haynes 282, developed for high-temperature applications in aero and land based gas turbine engines, is studied. Experiments for cyclic loading have been performed at room temperature and elevated temperature. To capture the cyclic hardening/softening of the material at the different temperatures, a plasticity model has been calibrated against experimental data. The robustness and the uniqueness of the identified material parameters are ensured by performing sensitivity and correlation analyses. A criterion based on the strain energy density, is used for LCF life predictions of Haynes 282. The criterion has been tuned to fit test data for the different temperatures and it has been evaluated with respect to both cyclic experimental data and with respect to model response. The influence of uncertainties in experimental data on identified material parameters, fatigue life predictions and finite element predictions has been investigated.

1 Introduction

In the aviation industry today there is a trend of increasing operating temperatures in turbine engines. This is due to the advantage in efficiency gained with higher temperatures, leading to improved performance. The demands of low weight and long life for the engine components are still important design issues. To be able to meet the challenging requirements of increasing temperature as well as those of low weight and long life, new efficient high temperature superalloys, such as Haynes 282 studied in this paper, are developed. However, to safely be able to use the full capacity of these superalloys, accurate modeling and simulation of the material behaviour during thermal and mechanical loading are needed.

Many constitutive models have been used to model the plastic and viscoplastic behaviour of metals. For overviews of these see e.g. Lemaitre and Chaboche (1990), Stouffer and Dame (1996), Chaboche (2008). For the modeling of the material behaviour of nickel-based superalloys recent work has been carried out by e.g. Becker and Hackenberg (2010), who developed a unified rate dependent and rate independent model able to cover the full temperature range of IN718 including the three creep stages. The constitutive behaviour of IN718 was also investigated by Gustafsson et al. (2011) with the aim of using a simple model with few material parameters to describe the initial softening of the material. Cornet et al. (2011) modeled the cyclic behaviour of Alloy RR1000 by a viscoplastic damage model. The multiaxial creep and cyclic plasticity in nickel-based superalloy C263 was modeled and compared to biaxial creep tests by Manonukul et al. (2005).

Two important aspects of Thermo-Mechanical Fatigue (TMF) in turbine applications can be identified. The accurate prediction of the material behaviour during the thermal and mechanical loading as well as the model used for life prediction. Many life prediction models for Low Cycle Fatigue (LCF) and TMF have been introduced in the literature. For overviews of these see e.g. Fatemi and Yang (1998), Cui (2002), Manson and Halford (2009).

In this paper an initial study of the cyclic behavior of the nickel-based superalloy Haynes 282 is presented. The material behaviour is modeled using a plasticity model originally formulated by Chaboche (1989) and the model predictions are compared to experimental results for uniaxial LCF tests at room temperature and 650°C. The identification of material parameters is based on the experimental data and formulated as a constrained optimization problem. The robustness and the uniqueness of the identified material parameters are ensured by performing sensitivity and correlation analyses. For the prediction of LCF life a criterion based on the strain energy density is used. The criterion is tuned to fit test data for the different temperatures and is evaluated with respect to both experimental data and with respect to model response.

2 Material Model

Many constitutive models have been used to characterize the phenomenological behavior of metals on the macroscale, see e.g. overviews by Lemaitre and Chaboche (1990), Stouffer and Dame (1996), Chaboche (2008). For super-alloys, used in turbine applications, the constitutive model should be able to mimic phenomena such as cyclic hardening, the Bauschinger effect, ratchetting, shake down, creep and stress relaxation. Due to the high temperatures in turbine applications, the rate dependent phenomena are of great importance to give an adequate prediction of the material behaviour. However, in this paper we only consider a rate independent plasticity model that was originally formulated by Chaboche (1989). The reason for this is that, at the present time, no experimental results are available for Haynes 282 that give information about its rate dependent response.

In the model framework the stress is partitioned into a volumetric σ_{vol} and a deviatoric part $\boldsymbol{\sigma}_{\text{dev}}$ which are related, by assuming linear isotropic elasticity, to the volumetric and deviatoric parts of the elastic strain $\boldsymbol{\epsilon}_e$

$$\begin{aligned} \boldsymbol{\sigma} &= \boldsymbol{\sigma}_{\text{dev}} + \frac{1}{3}\sigma_{\text{vol}}\mathbf{I} \\ \boldsymbol{\sigma}_{\text{dev}} &= 2G\boldsymbol{\epsilon}_{e,\text{dev}} \\ \sigma_{\text{vol}} &= 3K_b\epsilon_{\text{vol}} \end{aligned} \tag{1}$$

where G is the shear modulus and K_b is the bulk modulus. The elastic part of the strain $\boldsymbol{\epsilon}_e$ is obtained from the total strain $\boldsymbol{\epsilon}$ by subtracting the plastic strain $\boldsymbol{\epsilon}_p$ and the thermal strain

$$\boldsymbol{\epsilon}_e = \boldsymbol{\epsilon} - \boldsymbol{\epsilon}_p - \alpha\Delta\Theta\mathbf{I} \tag{2}$$

where α is the thermal expansion coefficient and $\Delta\Theta$ is the temperature increase. Furthermore, the plastic yielding is assumed to be governed by the von Mises yield function

$$\Phi = \sqrt{\frac{3}{2}}|\boldsymbol{\sigma}_{\text{dev}} - \mathbf{B}| - (\sigma_y - \kappa) \tag{3}$$

where $\mathbf{B}$ is the back-stress (kinematic hardening), σ_y is the initial yield stress and κ is the drag-stress (isotropic hardening). According to the normality rule, the plastic strain is assumed to evolve in an associative fashion

$$\dot{\boldsymbol{\epsilon}}_p = \dot{\lambda}\frac{\partial\Phi}{\partial\boldsymbol{\sigma}} = \dot{\lambda}\sqrt{\frac{3}{2}}\frac{\boldsymbol{\sigma}_{\text{dev}} - \mathbf{B}}{|\boldsymbol{\sigma}_{\text{dev}} - \mathbf{B}|} \tag{4}$$

The evolution of isotropic and kinematic hardening are assumed to be of Voce (1955) and of Armstrong and Frederick (1966) type

$$\begin{aligned} \dot{\kappa} &= \dot{\lambda}H_{\text{iso}}\left(1 - \frac{\kappa}{\kappa_\infty}\right) \\ \dot{\mathbf{B}}_i &= \dot{\lambda}H_i\left(\sqrt{\frac{2}{3}}\frac{\boldsymbol{\sigma}_{\text{dev}} - \mathbf{B}}{|\boldsymbol{\sigma}_{\text{dev}} - \mathbf{B}|} - \frac{\mathbf{B}_i}{B_{\infty,i}}\right) \end{aligned} \tag{5}$$

and

$$\mathbf{B} = \sum_{i=1}^{\text{n}_\text{B}} \mathbf{B}_i \tag{6}$$

where H_{iso}, κ_∞, H_i and $B_{\infty,i}$ are material parameters and n_B is the number of back-stresses used to obtain the total back-stress $\mathbf{B}$. The plastic multiplier $\dot{\lambda}$ describes the amount of plastic strain rate and is, for the case of rate independent inelasticity, given by the Kuhn-Tucker loading/unloading conditions

$$\Phi\dot{\lambda} = 0, \quad \dot{\lambda} \geq 0, \quad \Phi \leq 0 \tag{7}$$

To expand the model to include rate dependence the loading/unloading conditions could easily be replaced by introducing an over-stress function (see e.g. Lemaitre and Chaboche (1990)).

3 Material and Experiments

3.1 Haynes 282

Haynes 282 alloy is a wrought, γ' strengthened superalloy that was commercialized in the fall of 2005. The alloy was developed to combine the properties of high-temperature strength and good fabricability. For these kinds of wrought γ' strengthened alloys the amount of γ' phase is the main key to both of these properties. In general, a high content of γ' phase, as for the R-41 and Waspaloy alloys, gives a material with high strength but not so good fabricability especially with regards to welding. On the other hand a low content of the γ' phase, such as for the 263 alloy, gives a material with good fabricability but a limited temperature application range due to loss of strength at high temperatures. Hence, the γ' level in the 282 alloy was optimized to give a good balance between strength and fabricability cf. Pike (2006), Pike (2008).

3.2 LCF-Experiments

Experimental data from 16 isothermal LCF tests of Haynes 282 were available for calibration of the material model and fatigue criterion. The experiments were conducted at Room Temperature (RT) and 650°C. The tests were performed in strain control with the strain ranges 0.45, 0.6, 1.0 and 2.0 % at a frequency of 0.5 Hz. All tests had an R-value of 0. The criterion for crack initiation was 25 % load drop from the stable hysteresis loop and the failure criterion was a 50 % load drop from the stable hysteresis loop.

For the identification of the material parameters in the material model, 4 experiments at RT and 4 experiments at 650°C with strain ranges of 1.0 and 2.0 % were used. All 16 experiments were used for calibration of the strain energy density fatigue criterion (described in Section 5).

4 Parameter Identification and Sensitivity Analysis

4.1 Objective Function

Calibration of any constitutive material model can be formulated as a constrained optimization problem, where the purpose is to get as good agreement, between experiment and model response, as possible. The minimization problem can be written as

$$\min_{\boldsymbol{\pi}\in\Omega} E(\boldsymbol{\pi}) \tag{8}$$

where $\boldsymbol{\pi}$ is the set of n material parameters to be optimized, Ω is the admissible parameter space and E is the objective function. The admissible parameter space Ω is defined as a rectangular region in $\mathbb{R}^n$

$$\Omega = \{\boldsymbol{\pi} \in \mathbb{R}^n | \pi_{i,\text{min}} \leq \pi_i \leq \pi_{i,\text{max}},\ i = 1, 2, ..., n\} \tag{9}$$

In the present paper we will only consider uniaxial strain-controlled experiments. Further, we assume that for experiment k there are $\bar{N}_k$ experimental observations that are collected in the set

$$\bar{\mathbf{R}}_k = \{\bar{\sigma}(\bar{t}_l),\ l = 1, 2, ..., \bar{N}_k\} \tag{10}$$

whereas the N_k predicted stresses, for a given $\boldsymbol{\pi}$, from the integration of the constitutive relations are collected in a set

$$\mathbf{R}_k = \{\sigma(\boldsymbol{\pi}, t_l),\ l = 1, 2, ..., N_k\} \tag{11}$$

Clearly, the simulations must be controlled in the same fashion as the tests. However, the number of experimental observations $\bar{N}_k$ are usually not the same as the number of predicted states N_k. The comparison between the experiment and the predicted model response requires that their values correspond to the same time. This is accomplished by interpolation of the predicted set

$$\mathbf{R}_k = \{\sigma(\boldsymbol{\pi}, t_l),\ l = 1, 2, ..., N_k\} \overset{interp.}{\rightsquigarrow} \mathbf{R}_{k,interp.} = \{\sigma(\boldsymbol{\pi}, \bar{t}_l),\ l = 1, 2, ..., \bar{N}_k\} \tag{12}$$

The objective function E_k for experiment k can now be calculated as the time weighted least-squares error

$$E_k(\boldsymbol{\pi}) = \frac{w_k}{\bar{t}_{\bar{N}_k} - \bar{t}_1} \Big(\sum_{l=1}^{\bar{N}_k} \big(\Delta\bar{t}_l \big| \sigma(\boldsymbol{\pi}, \bar{t}_l) - \bar{\sigma}(\bar{t}_l) \big| \big)^2 \Big)^{\frac{1}{2}} \tag{13}$$

with

$$\Delta\bar{t}_1 = \frac{\bar{t}_2 - \bar{t}_1}{2},\ \ \Delta\bar{t}_l = \frac{\bar{t}_{l+1} - \bar{t}_{l-1}}{2},\ \ \Delta\bar{t}_{\bar{N}_k} = \frac{\bar{t}_{\bar{N}_k} - \bar{t}_{\bar{N}_k - 1}}{2} \tag{14}$$

The weighting factor w_k should represent the relative importance of experiment k. The worst agreement between predictions and experiments for a given $\boldsymbol{\pi}$ defines $E_{\max}$, i.e.

$$E_{\max} = \max_{1 \le k \le K} E_k \tag{15}$$

The total objective function E is chosen as

$$E(\boldsymbol{\pi}) = E_{\max} + \frac{1}{K} \sum_{k=1}^{K} E_k(\boldsymbol{\pi}) \tag{16}$$

By this choice the calibration result depends on all tests, but with double weight on the experiment giving the worst result $E_{\max}$ for the current $\boldsymbol{\pi}$.

4.2 Sensitivity Analysis and Correlation Matrix

A sensitivity analysis is performed for two reasons. Firstly, the response sensitivity $\mathrm{d}\mathbf{R}_{k,interp.}/\mathrm{d}\pi_i$ is used in gradient based optimization algorithms. Secondly, it can be used as a measure for how the parameters effect the response and how the parameters correlate. The vectors of relative response sensitivity, $\mathbf{r}_i$ are calculated numerically (analytical derivations of the response sensitivity can be performed by following Mahnken and Stein (1996))

$$\mathbf{r}_i = \frac{\mathbf{R}(\pi_i + \Delta\pi_i) - \mathbf{R}(\pi_i)}{\Delta\pi_i}\pi_i,\ i = 1, 2, ..., n \tag{17}$$

where the response vector $\mathbf{R}$ is the collection of predicted states defined in Equation 11. When using several experiments a set of all responses can be formulated as

$$\mathbf{R}_{\text{tot}} = \{\mathbf{R}_1, ..., \mathbf{R}_K\} \tag{18}$$

whereby a total response sensitivity can be calculated as

$$\mathbf{r}_{\text{tot},i} = \frac{\mathbf{R}_{\text{tot}}(\pi_i + \Delta\pi_i) - \mathbf{R}_{\text{tot}}(\pi_i)}{\Delta\pi_i}\pi_i,\ i = 1, 2, ..., n \tag{19}$$

The correlation between the parameters can be measured by the correlation matrix $\mathbf{c}$, which is defined as

$$c_{ij} = \frac{\mathbf{r}_{\text{tot},i} \cdot \mathbf{r}_{\text{tot},j}}{|\mathbf{r}_{\text{tot},i}||\mathbf{r}_{\text{tot},j}|} = \cos(\Theta_{ij}) \tag{20}$$

where Θ_{ij} is the angle between $\mathbf{r}_i$ and $\mathbf{r}_j$. If the response sensitivities with regard to parameter i and parameter j are almost orthogonal then c_{ij} is close to 0. Thus, parameter i and j are not correlated. However, if c_{ij} is close to ± 1 then the parameters correlate. In such a case, either there is a need for more or different types of experimental results or the number of parameters is too large and should be reduced.

4.3 Optimization Algorithm

In order to increase the probability of finding the global minimum of the objective function and to device a systematic approach, the calibration strategy is divided into two steps. In the first step, we compute the objective function E for a number of parameter combinations (that cover the admissible parameter space Ω), with the purpose to find good initial guesses for the optimization algorithm. In the second step, a number of these initial guesses, yielding the lowest values of the objective function, are used and optimization is performed for each of them. The optimization is carried out by first, for a limited number of evaluations of the objective function, applying a direct search method Nelder-Mead simplex method cf. Nelder and Mead (1965) followed by iterations using the gradient based based Han-Powell method with Armijo line search (see e.g. Bertsekas (1995), Luenberger (1984)) until convergence. Convergence is defined as when the change of the objective function after an iteration step is smaller than a specified tolerance.

For the case when using several back-stresses in the model special care should be taken to the calibration of the hardening parameters. In the model it is possible to choose as many kinematic hardening equations as preferred. By increasing the number of back-stresses the model's ability to form a smooth transition between the elastic and inelastic region increases. The drawbacks are that the calibration process becomes more complex and that the model implementation becomes less computational efficient. In this paper a superposition of three equations of nonlinear kinematic hardening are used as recommended by Chaboche (1986). The first back-stress is used to give an initial high modulus at the onset of yielding, the second back-stress is used for the transient nonlinear segment and the third back-stress is used to give a constant hardening modulus at higher strain ranges.

4.4 Scatter in Experimental Data

A material model calibration should be conducted with the awareness of the scatter obtained in the experimental data. An analysis of the scatter in the experiments used for model calibration was performed, comparing four experiments at room temperature and four experiments at 650°C with strain ranges of 1.0 % and 2.0 % ($\text{exp}_{k,\text{RT},1\%}$, $\text{exp}_{k,\text{RT},2\%}$, $\text{exp}_{k,650°\text{C},1\%}$, $\text{exp}_{k,650°\text{C},2\%}$, k=1,2). For each experiment a separate set of material parameters ($\boldsymbol{\pi}_{k,\text{RT},1\%}$, $\boldsymbol{\pi}_{k,\text{RT},2\%}$, $\boldsymbol{\pi}_{k,650°\text{C},1\%}$, $\boldsymbol{\pi}_{k,650°\text{C},2\%}$, k=1,2) for the material model using n_B=1 and fixed values of parameters σ_y and E were obtained. The model response compared to experimental data are shown in Figures 1-2. The material parameter sets obtained for experiments with k=1 were chosen as references and the difference with respect to parameters in the sets with k=2 are shown in Figure 3. The scatter in experiments with respect to obtained parameter sets are in general larger for the experiments at elevated temperature.

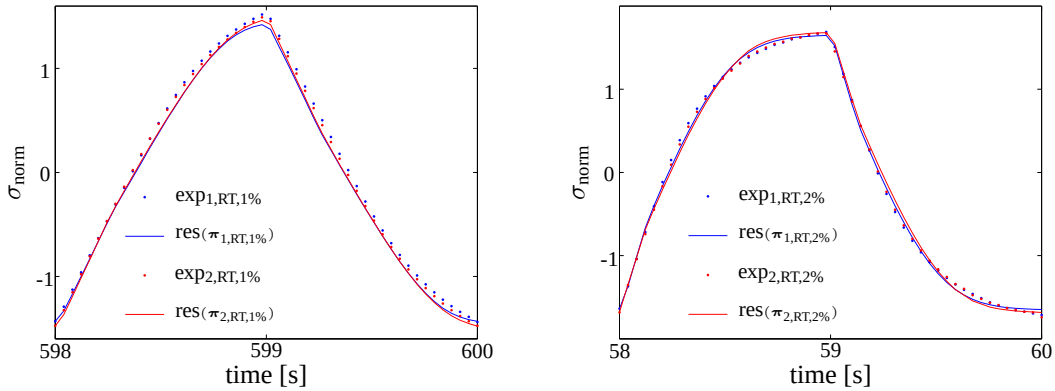

Figure 1: Experimental results and model response for stabilized hysteresis loop with respect to calibrated parameter sets for each experiment at RT and a) $\Delta\epsilon$=1 %, b) $\Delta\epsilon$=2 %.

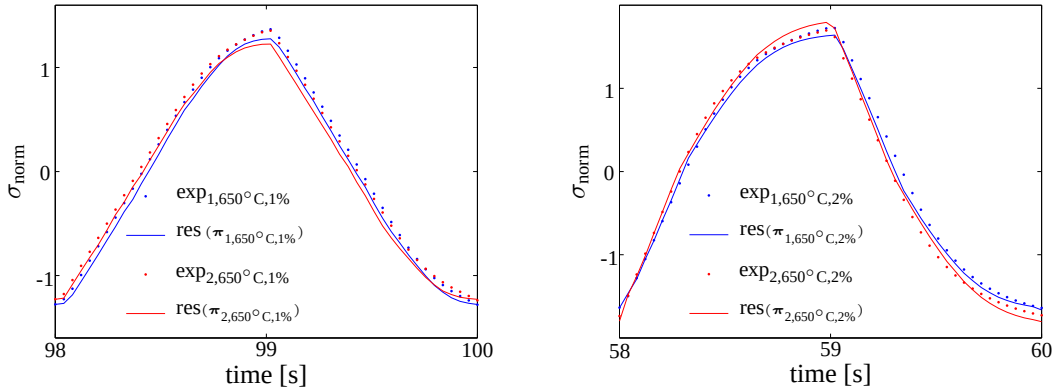

Figure 2: Experimental results and model response for stabilized hysteresis loop with respect to calibrated parameter sets for each experiment at 650°C and a) $\Delta\epsilon$=1 %, b) $\Delta\epsilon$=2 %.

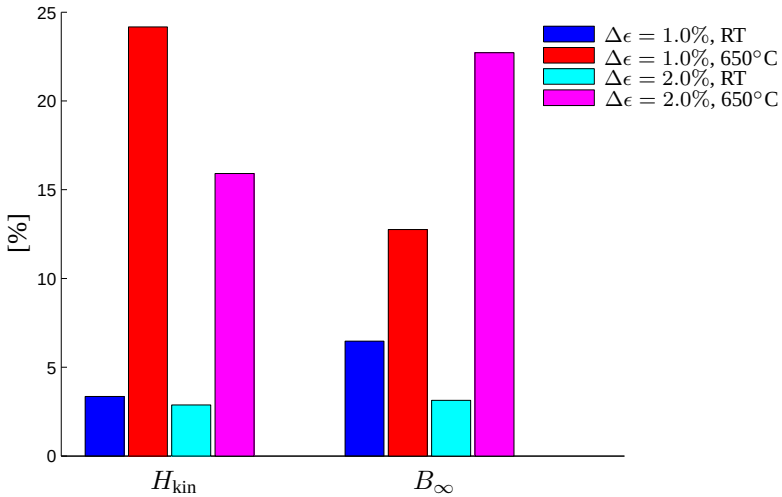

Figure 3: Difference in parameter values H_{kin} and B_∞ when comparing parameter sets ($\boldsymbol{\pi}_{k,\text{RT},1\%}$, $\boldsymbol{\pi}_{k,\text{RT},2\%}$, $\boldsymbol{\pi}_{k,650°\text{C},1\%}$, $\boldsymbol{\pi}_{k,650°\text{C},2\%}$, k=1,2) obtained from parameter identification with regard to experiments ($\text{exp}_{k,\text{RT},1\%}$, $\text{exp}_{k,\text{RT},2\%}$, $\text{exp}_{k,650°\text{C},1\%}$, $\text{exp}_{k,650°\text{C},2\%}$, k=1,2).

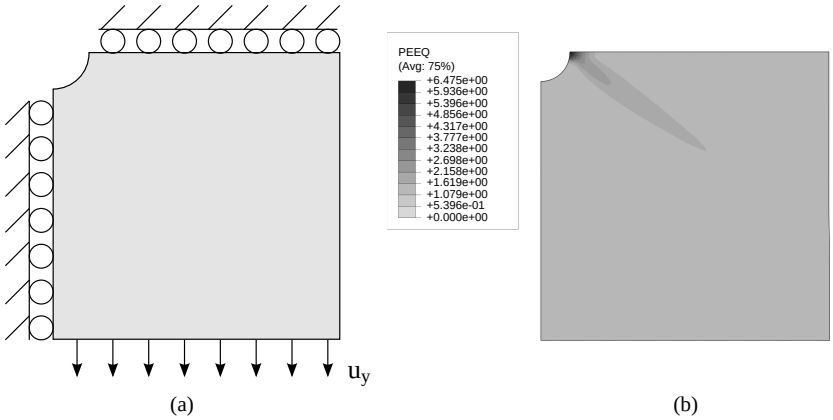

Figure 4: a) A schematic illustration of the simple FE problem, thin plate with a circular hole subjected to cyclic loading. b) Accumulated plastic strain obtained for $\boldsymbol{\pi}_{1,\mathrm{RT},1\%}$.

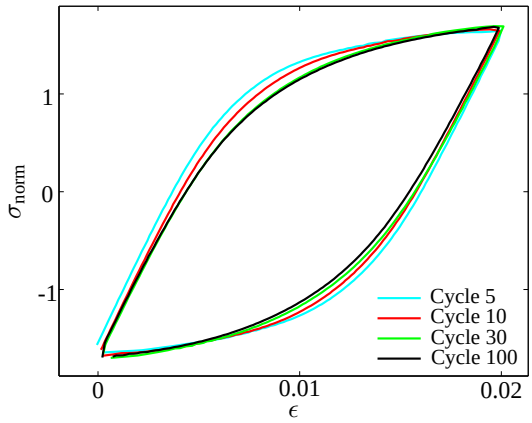

Figure 5: Stabilization of the hysteresis loops for $\mathrm{exp}_{1,\mathrm{RT},2\,\%}$.

The difference in model response due to scatter in experimental data was also investigated for a simple FE problem in the commercial FE code ABAQUS, see Figure 4. A thin plate with a circular hole was subjected to cyclic loading in terms of prescribed displacement u_y during 20 loading cycles. The maximum (in the plate) accumulated plastic strain $\lambda_{\max}$ obtained for each parameter set was then compared

$$\begin{aligned}\text{difference between } &\lambda_{\max}(\boldsymbol{\pi}_{1,\mathrm{RT},1\%}) \text{ and } \lambda_{\max}(\boldsymbol{\pi}_{2,\mathrm{RT},1\%}) = 9.73\% \\ &\lambda_{\max}(\boldsymbol{\pi}_{1,\mathrm{RT},2\%}) \text{ and } \lambda_{\max}(\boldsymbol{\pi}_{2,\mathrm{RT},2\%}) = 2.75\% \\ &\lambda_{\max}(\boldsymbol{\pi}_{1,650^\circ\mathrm{C},1\%}) \text{ and } \lambda_{\max}(\boldsymbol{\pi}_{2,650^\circ\mathrm{C},1\%}) = 5.19\% \\ &\lambda_{\max}(\boldsymbol{\pi}_{1,650^\circ\mathrm{C},2\%}) \text{ and } \lambda_{\max}(\boldsymbol{\pi}_{2,650^\circ\mathrm{C},2\%}) = 15.97\%\end{aligned} \tag{21}$$

Clearly, the difference would increase with the number of loading cycles and we can conclude that the influence of experimental scatter is significant.

4.5 Cyclic Model Response for Stabilized Hysteresis Loop

Since the experimental data used in this paper are classified, the numerical values of material parameters, model response and experimental results cannot be given explicitly. Instead the presented numerical values and results are normalized by a stress x_σ. It can be noted that the experiments showed no indications of isotropic hardening and hence this type of hardening is excluded from the model (i.e. $H_{\mathrm{iso}} = 0$). The LCF experiments for RT and 650°C all show that the material shake down to stabilized hysteresis loops. An example of this shakedown for an experiment at RT with $\Delta\epsilon = 2\%$ is shown in Figure 5. Two sets of parameters, one for the n_B=1 and one for

Θ	E/x_σ	σ_y/x_σ	H_{kin}/x_σ	B_∞/x_σ
20°C	4.44e2	6.72e-1	6.08e2	9.94e-1
650°C	3.44e2	9.00e-1	2.76e2	9.18e-1

Table 1: Normalized parameter sets for n_B=1 at RT and 650°C.

Θ	E/x_σ	σ_y/x_σ	H_1/x_σ	B_{∞_1}/x_σ	H_2/x_σ	B_{∞_2}/x_σ	H_3/x_σ	B_{∞_3}/x_σ
20°C	4.44e2	6.72e-1	3.52e2	3.00e-1	3.38e2	6.88e-1	2.20e0	∞
650°C	3.44e2	9.00e-1	3.16e3	1.20e-1	2.08e2	9.00e-1	2.40e0	∞

Table 2: Normalized parameter sets for n_B=3 at RT and 650°C.

n_B=3 were identified separately for RT and for 650°C, see Table 1 and 2. The model responses for the identified values of the material parameters are compared to experimental data in Figure 6. As can be observed in Figure 6, the material model is both for n_B=1 and n_B=3 able to capture the cyclic behaviour of Haynes 282 rather well for a stabilized hysteresis loop. The improvement when using n_B=3 compared to n_B=1 is fairly small (for this set of experimental data).

The difference in model response when using n_B=1 and n_B=3 was also investigated for a simple FE problem, see Figure 4(a). A thin plate with a circular hole was subjected to cyclic loading in terms of prescribed displacement u_y during 20 loading cycles. The resulting maximum accumulated plastic strain λ_{max} were then compared for simulations with $n_B = 1$ and $n_B = 3$. The result showed 5.8 % difference in max accumulated plastic strain at RT and 6.8 % difference at 650°C. Clearly, the difference would increase with the number of loading cycles and it can be expected that the difference would be significant in a gas-turbine application. However, these differences are comparable to differences in maximum accumulated plastic strain obtained in the analysis of the influence of scatter in experimental data (see Section 4.4).

4.5.1 Sensitivity Analysis and Correlation Matrix for Identified Material Parameter Sets

For the parameter sets obtained during the calibration process response sensitivities $\mathbf{r}_i$ and correlation matrices c_{ij} were computed. Sensitivities with respect to E, σ_y, H_{kin} and B_∞ for the model with n_B=1 can bee seen in Figure 7 for RT and in Figure 8 for 650°C. Corresponding correlation matrices are given in Table 3 for RT and Table 5 for 650°C. Sensitivities with respect to σ_y, $B_{\infty,1}$, H_2 and $B_{\infty,2}$ for the model with n_B=3 are shown in Figure 9 with corresponding correlation matrix in Table 4 for RT and in Figure 10 and Table 6 for 650°C. It can be seen that the influence of the different hardening terms, when using n_B=3, is separated since the correlation between these parameters is low. Note that, for illustration purposes, the sensitivities in Figures 7-10 have been scaled by each experiments maximum absolute value of the sensitivity.

5 Strain Energy Density Fatigue Criterion

Many life prediction models and criteria for LCF and TMF have been introduced in the literature. For overviews of these see e.g. Fatemi and Yang (1998), Cui (2002), Manson and Halford (2009). The particular choice of criterion depends on the material and the loading conditions. Hence, the criterion should be tested and evaluated for the material, temperature and loading intended for the application. As a first attempt to find a suitable fatigue criterion for the superalloy Haynes 282 a strain energy density criterion is chosen.

The strain energy density fatigue criterion used in this paper was introduced by Golos and Ellyin (1988). The total strain energy density ΔW_t, for a hysteresis loop, can be formulated as the sum of the plastic strain energy density

	E	σ_y	H_{kin}	B_∞
E	1.00	0.20	0.23	-0.61
σ_y	0.20	1.00	0.85	0.51
H_{kin}	0.23	0.85	1.00	0.32
B_∞	-0.61	0.51	0.32	1.00

Table 3: Correlation matrix of parameter sensitivity for model using n_B=1 at RT.

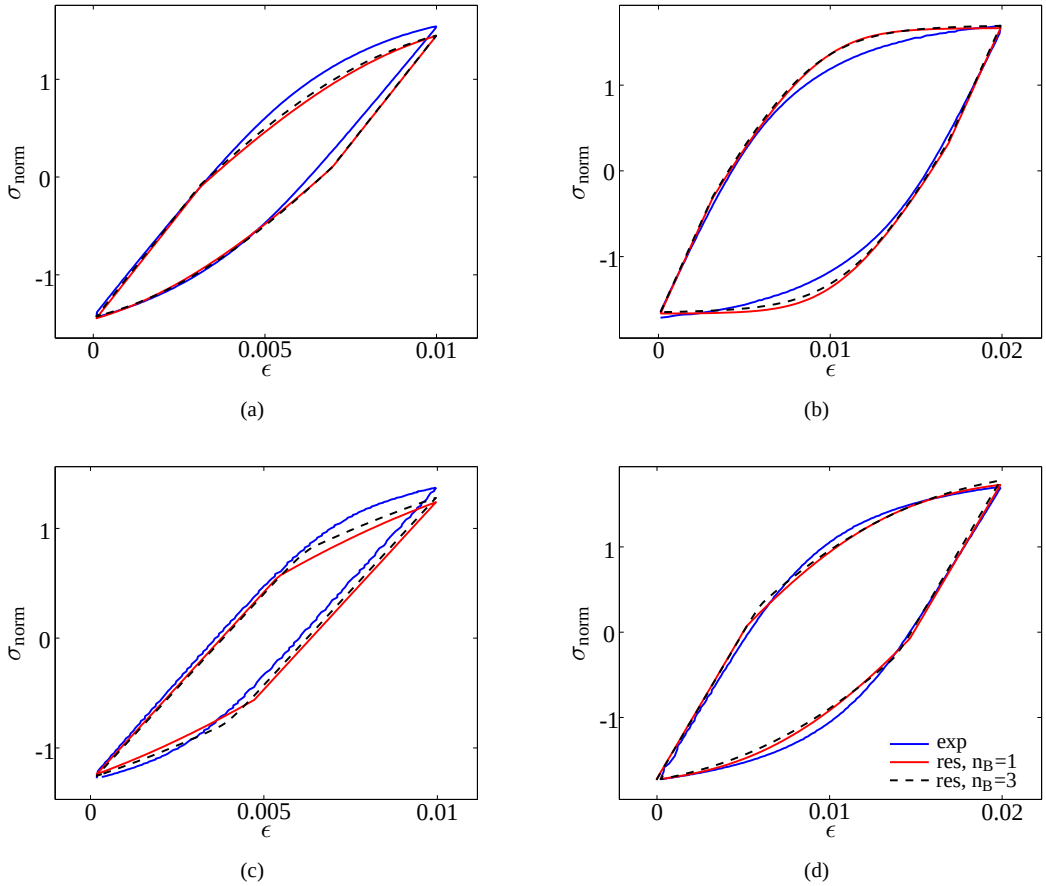

Figure 6: Calibrated model response compared to experimental results for, a) RT, $\Delta\epsilon$=1.0 % at cycle 300, b) RT, $\Delta\epsilon$=2.0 % at cycle 30, c) 650°C, $\Delta\epsilon$=1.0 % at cycle 50, d) 650°C, $\Delta\epsilon$=2.0 % at cycle 30.

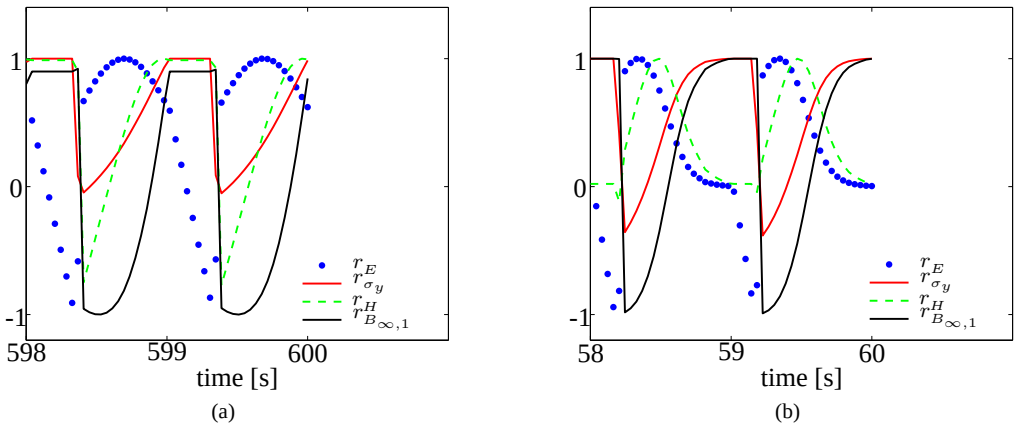

Figure 7: Scaled sensitivities with respect to E, σ_{y}, H_{kin} and B_{∞} for stable cycle of experiment a) $\mathrm{exp}_{1,\mathrm{RT},1\%}$ and b) $\mathrm{exp}_{1,\mathrm{RT},2\%}$.

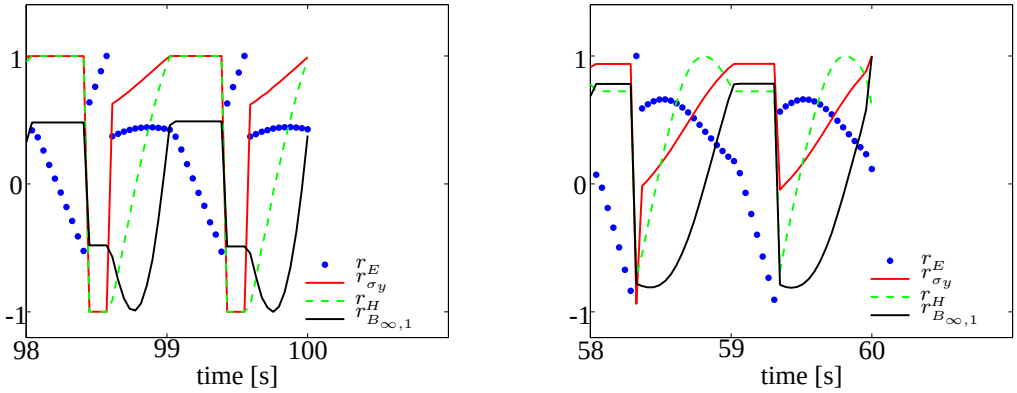

Figure 8: Scaled sensitivities with respect to E, σ_y, H_{kin} and B_∞ for stable cycle of experiment a) $\text{exp}_{1,650^\circ\text{C},1\%}$ and b) $\text{exp}_{1,650^\circ\text{C},2\%}$.

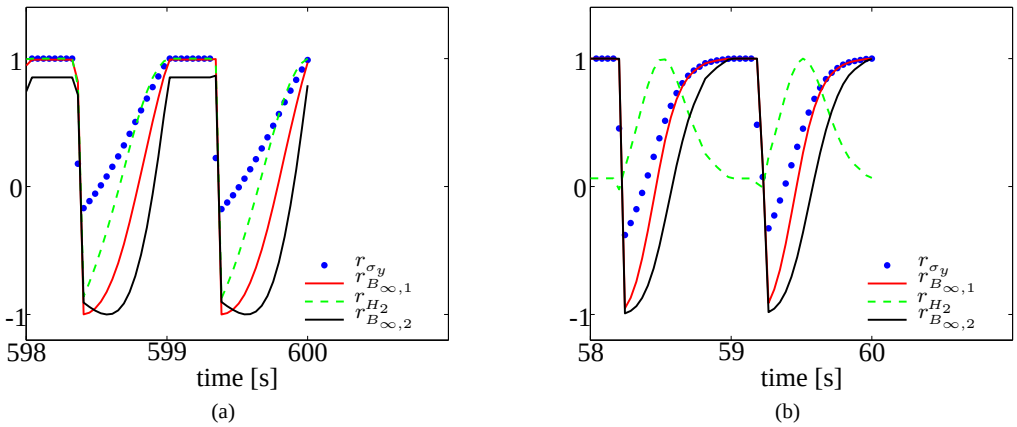

Figure 9: Scaled sensitivities with respect to σ_y, $B_{\infty,1}$, H_2 and $B_{\infty,2}$ for stable cycle of experiment a) $\text{exp}_{1,\text{RT},1\%}$ and b) $\text{exp}_{1,\text{RT},2\%}$.

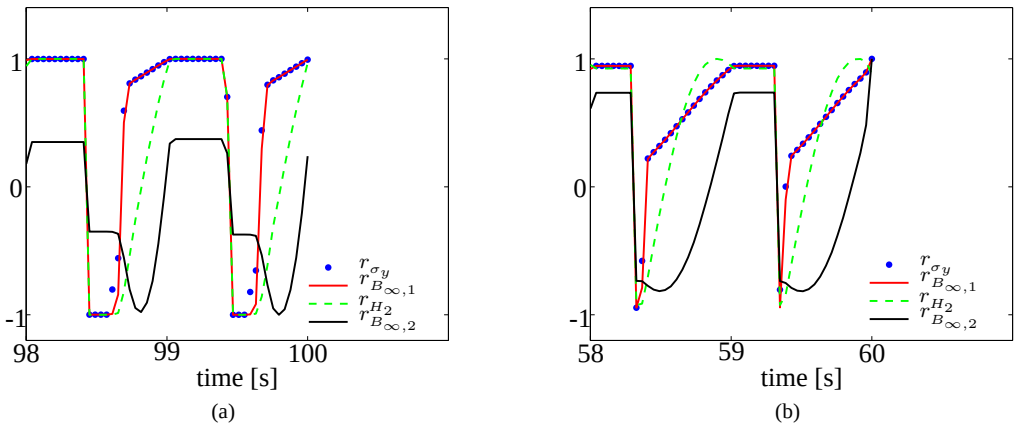

Figure 10: Scaled sensitivities with respect to σ_y, $B_{\infty,1}$, H_2 and $B_{\infty,2}$ for stable cycle of experiment a) $\text{exp}_{1,650^\circ\text{C},1\%}$ and b) $\text{exp}_{1,650^\circ\text{C},2\%}$.

	E	σ_y	H_1	B_{∞_1}	H_2	B_{∞_2}	H_3	B_{∞_3}
E	1.00	0.12	0.74	-0.49	-0.03	-0.65	-0.17	0.00
σ_y	0.12	1.00	0.60	0.75	0.86	0.45	0.14	0.00
H_1	0.74	0.60	1.00	0.00	0.47	-0.33	-0.06	0.00
B_{∞_1}	-0.49	0.75	0.00	1.00	0.80	0.80	0.22	0.00
H_2	-0.03	0.86	0.47	0.80	1.00	0.32	0.09	0.00
B_{∞_2}	-0.65	0.45	-0.33	0.80	0.32	1.00	0.27	0.00
H_3	-0.17	0.14	-0.06	0.22	0.09	0.27	1.00	0.00
B_{∞_3}	0.00	0.00	0.00	0.00	0.00	0.00	0.00	1.00

Table 4: Correlation matrix of parameter sensitivity for model using n_B=3 at RT.

	E	σ_y	H_{kin}	B_∞
E	1.00	-0.03	-0.10	-0.56
σ_y	-0.03	1.00	0.84	0.34
H_{kin}	-0.10	0.84	1.00	0.32
B_∞	-0.56	0.34	0.32	1.00

Table 5: Correlation matrix of parameter sensitivity for model using n_B=1 at 650°C.

	E	σ_y	H_1	B_{∞_1}	H_2	B_{∞_2}	H_3	B_{∞_3}
E	1.00	-0.15	0.41	-0.18	-0.29	-0.51	-0.17	0.00
σ_y	-0.15	1.00	-0.09	1.00	0.82	0.24	0.16	0.00
H_1	0.41	-0.09	1.00	-0.16	-0.25	-0.12	-0.06	0.00
B_{∞_1}	-0.18	1.00	-0.16	1.00	0.83	0.24	0.17	0.00
H_2	-0.29	0.82	-0.25	0.83	1.00	0.39	0.18	0.00
B_{∞_2}	-0.51	0.24	-0.12	0.24	0.39	1.00	0.34	0.00
H_3	-0.17	0.16	-0.06	0.17	0.18	0.34	1.00	0.00
B_{∞_3}	0.00	0.00	0.00	0.00	0.00	0.00	0.00	1.00

Table 6: Correlation matrix of parameter sensitivity for model using n_B=3 at 650°C.

ΔW_p and the positive part of the elastic strain energy density ΔW_e, see Figure 11. The reason for only using the positive part is that this part is correlated to crack opening and hence propagation in a high-cycle fatigue situation. According to Golos and Ellyin (1988) the relationship between fatigue life N_f and total strain energy density ΔW_t can be given as

$$\Delta W_t = \kappa N_f^{\alpha} + C \tag{22}$$

where κ, α and C are criterion parameters and N_f is the number of cycles to failure for loops with the total strain energy density ΔW_t.

The hysteresis loops in an LCF experiment are not identical, since first we have a shake down and at the end of the experiments the response change due to damage development. There can also be some variation in the assumed constant strain range in the experiments. To account for this in the criterion it should not be based solely on one single cycle but rather on all cycles in the experiment. Hence, all cycles are regarded as unique and a number of cycles to failure is obtained for the total strain energy of each cycle, n_i

$$N_{f_i} = \left(\frac{\Delta W_t(n_i) - C}{\kappa} \right)^{\frac{1}{\alpha}} \tag{23}$$

If the damage d_i of each cycle is assumed to be defined as $1/N_{f_i}$, then the total damage d_{tot} is obtained by using linear damage summation (according to the Palmgren-Miner rule)

$$d_{\text{tot}} = \sum_{i=1}^{I} d_i = \sum_{i=1}^{I} N_{f_i}^{-1} \tag{24}$$

or, more explicitly, by inserting Equation 23

$$d_{\text{tot}} = \sum_{i=1}^{I} \left(\frac{\Delta W_t(n_i) - C}{\kappa} \right)^{-\frac{1}{\alpha}} \tag{25}$$

Failure is assumed to occur when d_{tot}=1. To determine the criterion parameters, C, κ and α for RT as well as for 650°C the following objective function should be minimized

$$\min \sum_{k=1}^{K} \frac{1}{2} \left(d_{\text{tot},k}(C, \kappa, \alpha) - 1 \right)^2 \tag{26}$$

where $d_{\text{tot},k}$ is the obtained total damage for experiment k. The calibration of the criterion parameters are based on recorded hysteresis loops from the 16 LCF experiments for Haynes 282. Two experiments are available for each strain range and temperature. In Figure 12 the result of the best set of criterion parameters obtained for RT and 650°C are shown.

5.1 Predicted Fatigue Life

Since the experimental data used in this paper are classified, the numerical values of criterion parameters and criterion results as well as the experimental results cannot be given. Instead the results for the fatigue life are normalized by x_{N_f}. The predicted fatigue life based on experimental data $N_{f,\text{pre}}$ and predicted fatigue life based on simulated model response $N_{f,\text{sim}}$ using the model with n_B=1 and n_B=3 are compared to experimental results of fatigue life $N_{f,\text{exp}}$ in Figure 13. For RT the criterion is able to give a good prediction of fatigue life based on

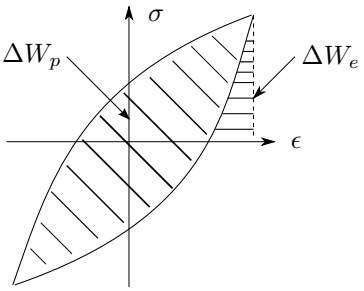

Figure 11: Schematic illustration of plastic and elastic strain energy density.

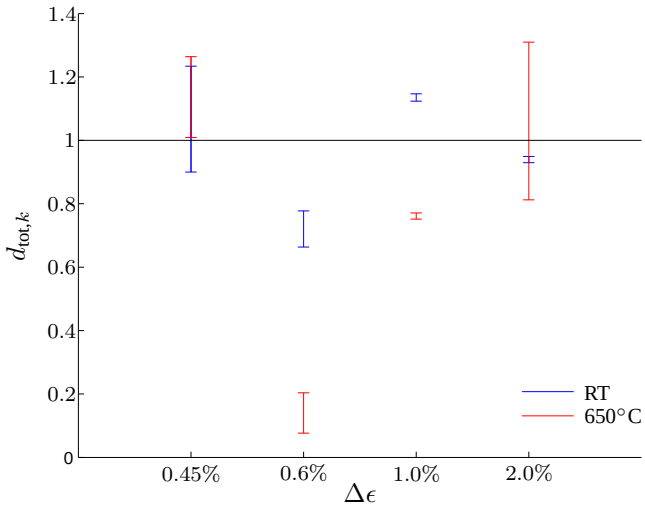

Figure 12: Result of total damage d_{tot} for calibrated fatigue criterion at RT and 650°C.

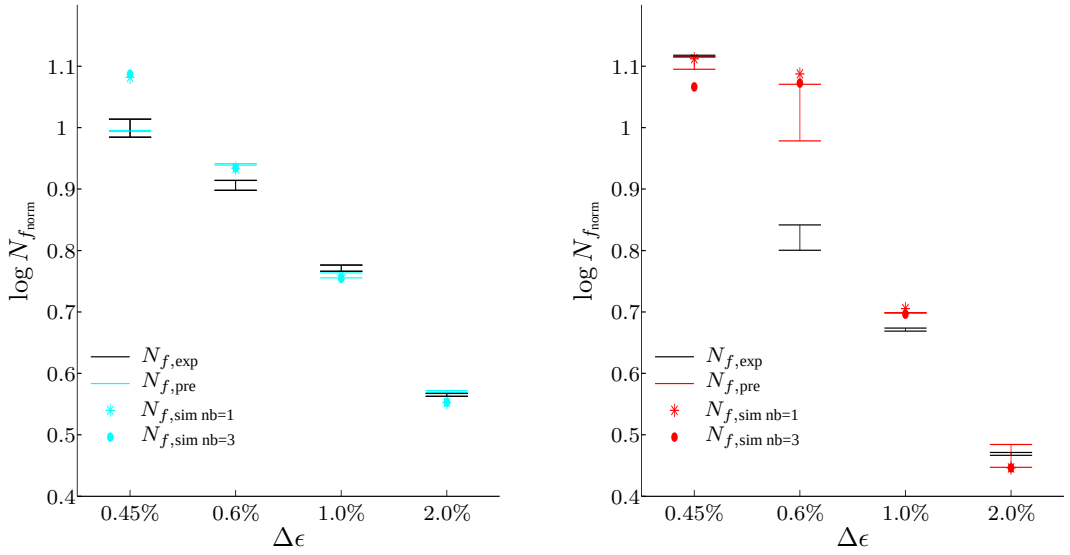

(a) (b)

Figure 13: Predicted fatigue life at a) RT and b) 650°C based on experiments $N_{f,\text{pre}}$ and simulated response $N_{f,\text{sim}}$ compared to experimental results of fatigue life $N_{f,\text{exp}}$.

the hysteresis loops of the experiment. However, for results based on the simulated model response it can be seen that the prediction of fatigue life is worse outside the strain range region for which the material model has been calibrated. As for the temperature of 650°C the criterion fails to give a sufficiently accurate prediction of fatigue life for strain ranges of 0.6 % and 1.0 %. For both RT and 650°C the difference obtained in predicted fatigue life based on simulated model response when using the model with n_B=1 and n_B=3 can be considered to be small.

6 Conclusions

The challenging requirements of increasing temperatures as well as low weight and long life for future gas-turbine components raises the demands on accurate modeling and simulation of the material behaviour. In this paper the cyclic behaviour of the nickel-based superalloy Haynes 282 at RT and 650°C was investigated. The material behaviour was modeled by a plasticity model originally formulated by Chaboche (1989). The model includes nonlinear kinematic hardening of Armstrong-Frederick type and possible superposition of several hardening terms (back-stresses). Material parameter identifications based on uniaxial LCF tests were carried out for the cases of using 1 back-stress and 3 back-stresses, respectively. It was shown that the material model was, both for n_B=1 and n_B=3, able to describe the cyclic behaviour of Haynes 282 for stabilized hysteresis loops rather well. However, the enhancement when using n_B=3 compared to n_B=1 was fairly small (for the given set of experimental data).

The responses of the model when using n_B=1 and n_B=3 were also compared for a simple FE problem, consisting of a thin plate with a circular hole subjected to cyclic loading, in the commercial code ABAQUS. The difference in maximum accumulated plastic strain obtained when using n_B=1 and n_B=3 indicates that the difference could be significant e.g. for a gas-turbine application subjected to many loading cycles. Nevertheless, the difference is not larger then the difference we would obtain in the simulations due to uncertainties in the identified material parameters as a result of scatter in experimental data.

A strain energy density fatigue criterion, originally introduced by Golos and Ellyin (1988), was calibrated with respect to experimental data and then used for prediction of the LCF life. It was observed that the fatigue criterion gave a rather good prediction of the fatigue life based on the hysteresis loops of the experiments at RT. However, the criterion could not be fitted with sufficiently accuracy to experiments (with different strain amplitudes) at 650°C.

7 Acknowledgments

The authors are grateful to Dr. Johan Olsson for valuable discussions. The work has been founded by the Swedish National Aeronautical Research Program (NFFP).

References

Armstrong, P.; Frederick, C.: A mathematical representation of the multiaxial Bauschinger effect. *Report RD/B/N/731, Central Electricity Geneating Board, Berkely UK, (1966)*.

Becker, M.; Hackenberg, H.: A constitutive model for rate dependent and rate independent inelasticity. application to IN718. *International Journal of Plasticity*, 27, (2010), 596 – 619.

Bertsekas, D.: *Nonlinear Programming*. Athena Scientific, Belmont, Massachusetts (1995).

Chaboche, J.: Time-independent constitutive theories of cyclic plasticity. *International Journal of Plasticity*, 2, (1986), 149 – 188.

Chaboche, J.: Constitutive equations for cyclic plasticity and cyclic viscoplasticity. *International Journal of Plasticity*, 5, (1989), 247 – 302.

Chaboche, J.: A review of some plasticity and viscoplasticity constitutive theories. *International Journal of Plasticity*, 24, (2008), 1642 – 1693.

Cornet, C.; Zhao, L.; Tong, J.: A study of cyclic behaviour of a nickel-based superalloy at elevated temperature using a viscoplastic-damage model. *International Journal of Fatigue*, 33, (2011), 241 – 249.

Cui, W.: A state-of-the-art review on fatigue life prediction methods for metal structures. *Jornal of Marine Science and Technology*, 7, (2002), 43 – 56.

Fatemi, A.; Yang, L.: Cumulative fatigue damage and life prediction theories: A survey of the state of the art for homogeneous materials. *International Journal of Fatigue*, 20, (1998), 9 – 34.

Golos, K.; Ellyin, F.: A total strain energy density theory for cumulative fatigue damage. *Journal of Pressure Vessel Technology*, 110, (1988), 36 – 41.

Gustafsson, D.; Moverare, J.; Simonsson, K.; Sjöström, S.: Modeling of the constitutive behavior of Inconel 718 at intermidiate temperatures. *Journal of Engineering for Gas Turbines and Power*, 133, (2011), –.

Lemaitre, J.; Chaboche, J.: *Mechanics of solid materials*. Cambridge University Press, Cambridge (1990).

Luenberger, D.: *Linear and nonlinear Programming, 2nd Edition*. Addison-Wesley Inc., Reading, Massachusetts (1984).

Mahnken, R.; Stein, E.: Parameter identification for viscoplastic models based on analytical derivatives of a least-squares functional and stability investigations. *International Journal of Plasticity*, 12, (1996), 451 – 479.

Manonukul, A.; Dune, F.; Knowles, D.; Williams, S.: Multiaxial creep and cyclic plasticity in nickel-base superalloy C236. *International Journal of Plasticity*, 21, (2005), 1 – 20.

Manson, S.; Halford, G.: *Fatigue and Durability of Metals at High Temperatures*. ASM International, Ohio (2009).

Nelder, J.; Mead, R.: A simplex method for function minimization. *Computer Journal*, 7, (1965), 308 – 313.

Pike, L.: Haynes 282 alloy - a new wrougth superalloy designed for improved creep strength and fabricability. *Proceedings of the ASME Turbo Expo*, 4, (2006), 1031 – 1039.

Pike, L.: Development of a fabricable gamma-prime (γ') strengthened superalloy. *Proceedings of the International Symposium on Superalloys*, -, (2008), 191 – 200.

Stouffer, D.; Dame, L.: *Inelastic deformation of metals : models, mechanical properties, and metallurgy*. Wiley and Sons, Inc., New York (1996).

Voce, E.: A practical strain hardening function. *Metallurgica*, 51, (1955), 219 – 226.

Address: Rebecka Brommesson and Magnus Ekh, Department of Applied Mechanics, Division of Material and Computational Mechanics, Chalmers University of Technlogy, Gothenburg.
email: rebecka.brommesson@chalmers.se; magnus.ekh@chalmers.se